Simulation of Electrohydrodynamic Enhancement of Laminar Flow Heat Transfer

GEORGE S. DULIKRAVICH, VINEET AHUJA

Department of Aerospace Engineering, The Pennsylvania State University, University Park, Pennsylvania, USA 16802

SEUNGSOO LEE

Research Scientist, Agency for Defense Development, Taejon, Korea

A mathematical model for laminar steady flow of an incompressible, viscous, neutrally-charged carrier fluid mixed with a fluid having electrically charged particles is presented. Thermally induced buoyancy was incorporated via an extended Boussinesq approximation allowing for temperature-dependent density, viscosity, heat conductivity and heat capacity while including Joule heating and electroconvective motions due to Lorentz forces. Induced magnetic fields and viscous dissipation in energy conservation equation have been neglected. Viscosity was modeled as a function of local electrical charge concentration thus simulating particle chaining phenomena in electrorheological fluids. Numerical results clearly demonstrate the influence that an applied electrostatic field and the consequent electric charge gradients can have on the flow pattern, temperature field and surface convective heat fluxes.

Key Words: *Heat Transfer; Electrohydrodynamics; Convection; Numerical methods;* CFD

E lectrohydrodynamics (EHD) and magnetohydrodynamics (MHD) represent two extreme models for a fluid flow under the influence of a combined electromagnetic field (Landau and Lifshitz, 1960; Eringen and Maughin, 1990a, 1990b). The EHD model assumes a quasi-static electric field applied to a fluid containing electrically charged particles and having negligible magnetic induction effects (Stuetzer, 1962; Melcher, 1981; Babski *et al.*, 1989), while the MHD model assumes that there are no charged particles in the flow field (Stuetzer, 1962).

The phenomenon of electrohydrodynamic instability or the generation of vorticity resulting from a non-uniform electric charge distribution in the fluid under the influence of an electric field is well known (Landau and Lifshitz, 1960; Ostroumov, 1966). The mechanism of electric charge injection offers a process wherein continuous work is done in convecting the flow by the release of electrical potential energy. The injection of charges between two electrodes and special cases of charging transients to a step voltage or current source for space charge limited conditions at the injecting electrode along with discharging transients were dealt in detail by Zahn and Chatelon (1977).

The EHD enhancement of heat transfer has been demonstrated by Fujino *et al.* (1989) for flows between parallel plates. Investigations carried out by Fernandez and Poulter (1987) have also revealed the enhancement of heat transfer rates exhibited by liquids flowing in ducts when subjected to an electrostatic potential. A comprehensive review of the operational principles of the EHD in single phase and phase-change heat exchangers is provided by Ohadi (1991). Nevertheless, only incomplete models of EHD flows have been numerically solved in the past (Belo and Polezhaev, 1991; Lee, Dulikravich and Kosovic, 1991). The main reason is the extreme complexity of the mathematical models (Babski *et al.*, 1989).

One of the least understood phenomena is that under the influence of an applied electric field the charged particles will start connecting and forming chains between electrodes (Korobko and Mokeev,

1991) with the distribution of these chains being random. This leads to an increase in the effective fluid viscosity of several orders of magnitude. Actually, it has been observed that the electrorheological fluid can become an effective solid (Tao and Sun, 1991; Tao, 1992) if a very high electric potential difference is applied across a very narrow region filled with such a fluid.

Several attempts to develop a comprehensive mathematical model for the relationship between the effective viscosity and the electrical field parameters in such fluids have been made (Korobko and Mokeev, 1991; Tao and Sun, 1991; Tao, 1992; Hosseini-Sianaki *et al.*, 1992; Usman *et al.*, 1992). Nevertheless, none of the models seem to be simple and reliable enough to effectively demonstrate the effect of increased viscosity on convective heat transfer in such fluids.

This paper attempts to demonstrate the significant influence that this fundamental phenomena has on heat transfer enhancement. A detailed numerical investigation of the impact of the EHD phenomenon on the distribution of surface heat fluxes and the influence of charge injection pattern on the enhancement of heat transfer is also carried out.

MATHEMATICAL MODEL

The mathematical model presented in this paper consists of an electrically neutral, homocompositional, viscous, incompressible carrier fluid that is seeded with one specie of charged particles having all physical properties identical to those of the carrier fluid except that the particles are electrically charged. This model can be extended to electrically non-neutral carrier fluids and multiple-specie particles having different physical properties. One possibility for creating such a model is to use concepts of mixture theory (Usman *et al.*, 1992). In this paper the objective is to demonstrate only fundamental effects of the applied electrostatic field for which a single-specie formulation will suffice. Although most practical heat exchangers work with turbulent flows, we have decided to study EHD effects in laminar flows since reliable and universal turbulence models for EHD flows do not exist. We will also assume that there is no electrolysis and no pool boiling.

The system of governing equations for EHD can be derived from a combination of Maxwell's equations of electrodynamics and the Navier-Stokes equations (Lee, Dulikravich and Kosovic, 1991; Lee, Dulikravich

and Ahuja, 1993). An idealized charged fluid is assumed (Stuetzer, 1962; Melcher, 1981) and, therefore, induced magnetic fields can be neglected. The magnetic field vector and the electric polarization vector are assumed negligible compared to the electric field vector so that Maxwell's equations can be reduced to an electric charge conservation equations and a Poisson's partial differential equation for electric potential since the electric field is irrotational. Here, it was assumed that ε is constant. Non-dimensionalization can be performed with respect to the reference values denoted by subscript o, so that

$$\mathbf{v}^* = \frac{\mathbf{v}}{v_o} \quad \mathbf{x}^* = \frac{\mathbf{x}}{l_o} \quad t^* = \frac{tv_o}{l_o} \quad p^* = \frac{p}{\rho_o v_o^2} \qquad (1)$$

$$\varphi^* = \frac{\Delta\varphi}{\Delta\varphi_o} \quad \mathbf{E}^* = \frac{\mathbf{E}l_o}{\Delta\varphi_o} \quad q^* = \frac{q}{q_o} \quad \theta = \frac{\Delta T}{\Delta T_o} \quad \mathbf{g}^* = \frac{\mathbf{g}}{g_o} \qquad (2)$$

If T_c is the temperature of the cold wall and T_h is the temperature of the hot wall, then $\Delta T = T - T_c$ and $\Delta T_o = T_h - T_c$. Similarly, $\Delta\varphi_o$ is the reference value of the electric potential difference between the two wall electrodes. Fluid density, electric charge mobility and coefficients of specific heat, thermal expansion, viscosity and heat conduction can be expressed as arbitrary functions of non-dimensional temperature (Gray and Giorgini, 1976; Lee, Dulikravich and Kosovic, 1991)

$$\rho = \rho_o \rho'(\theta) \quad b = b_o b'(\theta) \quad c = c_o c'(\theta) \qquad (3)$$

$$\alpha = \alpha_o \alpha'(\theta) \quad \eta = \eta_o \eta'(\theta) \quad k = k_o k'(\theta) \qquad (4)$$

We can now introduce non-dimensional numbers (Lee, Dulikravich and Kosovic, 1991) defined as

Reynolds number

$$Re = \frac{\rho_o v_o l_o}{\eta_o}$$

Prandtl number

$$Pr = \frac{c_o \eta_o}{k_o} \qquad (5)$$

Grashof number

$$Gr = \frac{\rho_o^2 g_o \alpha_o \Delta T_o l_o^3}{\eta_o^2}$$

Eckert number

$$Ec = \frac{v_o^2}{c_o \Delta T_o} \qquad (6)$$

Froude number

$$Fr^2 = \frac{v_o^2}{g_o l_o} \qquad (7)$$

Charge diffusivity number

$$D_E = \frac{\eta_0}{\rho_0 D_0}$$

Lorentz force number

$$S_E = \frac{q_0 \Delta\varphi_0}{\rho_0 v_0^2} \qquad (8)$$

Electric Prandtl number

$$Pr_E = \frac{\eta_0}{\rho_0 b_0 \Delta\varphi_0}$$

Electric field number

$$N_E = \frac{q_0 l_0^2}{\varepsilon \Delta\varphi_0} \qquad (9)$$

The electric charge diffusivity coefficient D and charge mobility coefficient b are related by Einstein's formula (Babski et al., 1989)

$$D = \frac{k_B T}{q m_i} \rho_i b \qquad (10)$$

where m_i is the mass of charged particle and ρ_i is the density of the electrically charged fluid. The non-dimensional density ρ' can be expanded in a Taylor series while retaining only the first order term

$$\rho' = 1 - \alpha\Delta T = 1 - \alpha^* \theta \qquad (11)$$

where

$$\alpha^* = \frac{\partial\rho'}{\partial\theta} = \frac{\partial\rho'}{\partial\theta}\frac{\Delta T_o \rho_o}{\rho_o \Delta T_o} = \frac{1}{\rho_o}\frac{\partial\rho}{\partial T}\Delta T_o = \alpha\Delta T_o \qquad (12)$$

It can be assumed that the coefficient of thermal expansion, α, is constant in the range of temperatures which are of interest in a particular case. Starting with the complete Navier-Stokes equations for compressible fluid flow and assuming that $(\alpha\Delta T_o) \ll 1$, an extended form of the Boussinesq approximation can be derived for the fluids with temperature-dependent properties (Gray and Giorgini, 1976; Lee, Dulikravich and Kosovic, 1991). Thus, the non-dimensional system of equations for incompressible flow of a fluid with temperature-dependent properties and containing electric charges under the influence of an electrostatic field can be reduced (Lee, Dulikravich and Kosovic, 1991) to

$$\nabla^* \cdot \mathbf{v}^* = 0 \qquad (13)$$

$$\frac{\partial\mathbf{v}^*}{\partial t^*} + \nabla^* \cdot (\mathbf{v}^*\mathbf{v}^* + \bar{p}^*\mathbf{I}) = \frac{1}{Re}\nabla^* \cdot (\eta' \nabla^*\mathbf{v}^*)$$

$$+ \frac{Gr\theta}{Re^2}\mathbf{g}^* + S_E q^*\mathbf{E}^* \qquad (14)$$

$$\frac{\partial\theta}{\partial t^*} + \nabla^* \cdot (\theta^*\mathbf{v}^*) = \frac{1}{Pr Re c'}\nabla^* \cdot (k'\nabla^*\theta)$$

$$+ \frac{S_E Ec}{c'}\left(q^*\left(\mathbf{v}^* + \frac{\mathbf{E}^*}{Re Pr_E}\right) - \frac{\nabla^* q^*}{Re D_E}\right) \cdot \mathbf{E}^* \qquad (15)$$

$$\frac{\partial q^*}{\partial t^*} + \nabla^* \cdot \left(q^*\left(\mathbf{v}^* + \frac{\mathbf{E}^*}{Re Pr_E}\right)\right)$$

$$= \frac{1}{Re}\nabla^* \cdot \left(\frac{b'}{D_E}\nabla^* q^*\right) \qquad (16)$$

$$\nabla^{*2}\varphi^* = -N_E q^* \qquad (17)$$

where $\bar{p}^* = p^* + \phi^*/Fr^2$ is a combination of hydrostatic and hydrodynamic pressure so that $\mathbf{g}^* = \nabla^*\phi^*$. According to the Boussinesq approximation, viscous dissipation can be neglected (Gray and Giorgini, 1976; Lee, Dulikravich and Kosovic, 1991) since its ratio with respect to the convective term in the energy equation is of the order Ec/Re which is typically a very small number.

NUMERICAL MODEL

For simplicity and clarity of notation, the asterisk symbol in the system of Eqs. (13–17) will be omitted. The system (13–16) can then be written in a fully conservative vector form in physical Cartesian coordinates as follows

$$\frac{\partial\mathbf{Q}}{\partial t} + \frac{\partial\mathbf{E}}{\partial x} + \frac{\partial\mathbf{F}}{\partial y} = \frac{\partial}{\partial x}\left(\mathbf{D}\frac{\partial\mathbf{Q}}{\partial x}\right) + \frac{\partial}{\partial y}\left(\mathbf{D}\frac{\partial\mathbf{Q}}{\partial y}\right) + \mathbf{S} \qquad (18)$$

where the solution vector $\mathbf{Q}$ and the flux vectors $\mathbf{E}$, $\mathbf{F}$ are defined as

$$\mathbf{Q} = \begin{Bmatrix} 0 \\ u \\ v \\ \theta \\ q \end{Bmatrix} \quad \mathbf{E} = \begin{Bmatrix} u \\ u^2 + \bar{p} \\ uv \\ u\theta \\ q\left(u + \frac{E_x}{Re Pr_E}\right) \end{Bmatrix}$$

$$\mathbf{F} = \left\{ \begin{array}{c} v \\ vu \\ v^2 + \bar{p} \\ v\theta \\ q\left(v + \dfrac{E_y}{Re\,Pr_E}\right) \end{array} \right\} \tag{19}$$

$$\mathbf{S} = \left\{ \begin{array}{c} 0 \\ \dfrac{Gr}{Re^2}\,\theta\,g_x + S_E q E_x \\ \dfrac{Gr}{Re^2}\,\theta\,g_y + S_E q E_y \\ \dfrac{S_E E_c}{c'}\left(q\left(\mathbf{v} + \dfrac{\mathbf{E}}{Re Pr_E}\right) - \dfrac{\nabla q}{Re D_E}\right) \cdot \mathbf{E} \\ 0 \end{array} \right\}$$

$$\mathbf{D} = \dfrac{1}{Re} \left\{ \begin{array}{c} 0 \\ \eta' \\ \eta' \\ \dfrac{k'}{Pr c'} \\ \dfrac{b'}{D_E} \end{array} \right\}^T \tag{20}$$

For the purpose of developing a versatile EHD analysis code applicable to arbitrary configurations where correct boundary conditions could be easily enforced precisely at the boundaries, the system of equations governing EHD flows was transformed in a fully conservative vector form in general ξ, η, curvilinear boundary-conforming non-orthogonal coordinates (Lee, Dulikravich and Kosovic, 1991; Lee, Dulikravich and Ahuja, 1993) as

$$\frac{\partial \tilde{\mathbf{Q}}}{\partial t} + \frac{\partial \tilde{\mathbf{E}}}{\partial \xi} + \frac{\partial \tilde{\mathbf{F}}}{\partial \eta} = \frac{\partial}{\partial \xi}\left(\frac{\tilde{\mathbf{D}}}{J}\,g_{ij}\,\frac{\partial J\tilde{\mathbf{Q}}}{\partial \xi}\right)$$

$$+ \frac{\partial}{\partial \eta}\left(\frac{\tilde{\mathbf{D}}}{J}\,g_{ij}\,\frac{\partial J\tilde{\mathbf{Q}}}{\partial \eta}\right) + \tilde{\mathbf{S}} \tag{21}$$

where

$$\tilde{\mathbf{Q}} = \frac{1}{J}\left\{ \begin{array}{c} \bar{p}/\beta \\ u \\ v \\ \theta \\ q \end{array} \right\} \qquad \tilde{\mathbf{E}} = \frac{1}{J}\left\{ \begin{array}{c} U \\ Uu + \xi_{,x}\,\bar{p} \\ Uv + \xi_{,y}\bar{p} \\ U\theta \\ q\left(U + \dfrac{E_\xi}{Re Pr_E}\right) \end{array} \right\}$$

$$\tilde{\mathbf{F}} = \frac{1}{J}\left\{ \begin{array}{c} V \\ Vu + \eta_{,x}\bar{p} \\ Vv + \eta_{,y}\,\bar{p} \\ V\theta \\ q\left(V + \dfrac{E_\eta}{Re\,Pr_E}\right) \end{array} \right\} \tag{22}$$

Here, $\tilde{\mathbf{S}} = \mathbf{S}$, $\tilde{\mathbf{D}} = \mathbf{D}$, $J = \partial(\xi, \eta)/\partial(x, y)$ and g_{ij} is the metric tensor given by $g_{ij} = \nabla x'_i \nabla x'_j$, while U, V are contravariant velocity vector components. A non-physical term, $\partial(\bar{p}/\beta)/\partial t$, representing an artificial compressibility (Chorin, 1967) was added so that the system (13–16) can be made non-singular and consequently integrated in time simultaneously. Parameter β is a user specified constant that depends on the Reynolds number and computational grid clustering, orthogonality and smoothness (Lee and Dulikravich, 1991b). The artificial compressibility concept is more consistent and easier to code than an equally common pressure-based algorithm for incompressible Navier-Stokes equations. The system of coupled nonlinear partial differential equations (21) was discretized using central differencing and integrated iteratively using a four-stage explicit Runge-Kutta time stepping (Jameson et al., 1981) given as

$$\tilde{\mathbf{Q}}^0 = \tilde{\mathbf{Q}}^n$$

$$\Delta\tilde{\mathbf{Q}}^m = -\gamma_m \Delta t\,\tilde{\mathbf{R}}^{m-1} \quad m = 1, 2, 3, 4 \tag{23}$$

$$\tilde{\mathbf{Q}}^{n+1} = \tilde{\mathbf{Q}}^n + \Delta\tilde{\mathbf{Q}}^4$$

where the iteration level is denoted by n, and each stage of the Runge-Kutta algorithm by m. Here the coefficients are $\gamma_m = 1/4, 1/3, 1/2$ and 1, respectively. The residual vector $\tilde{\mathbf{R}}$ is defined as

$$\tilde{\mathbf{R}} = \frac{\partial \tilde{\mathbf{E}}}{\partial \xi} + \frac{\partial \tilde{\mathbf{F}}}{\partial \eta} - \frac{\partial}{\partial \xi}\left(\frac{\tilde{\mathbf{D}}}{J}\,g_{ij}\frac{\partial J\tilde{\mathbf{Q}}}{\partial \xi}\right) - \frac{\partial}{\partial \eta}\left(\frac{\tilde{\mathbf{D}}}{J}\,g_{ij}\frac{\partial J\tilde{\mathbf{Q}}}{\partial \eta}\right) - \tilde{\mathbf{S}}$$

$$- \frac{\varepsilon_4\psi}{8J\Delta t}\left[\frac{\partial^4}{\partial \xi^4} + \frac{\partial^4}{\partial \eta^4}\right](J\tilde{\mathbf{Q}}) \tag{24}$$

The last term in this expression represents a fourth order artificial dissipation that was added explicitly to stabilize the algorithm which is otherwise prone to even-odd decoupling oscillations because it uses central differencing (Steger and Kutler, 1977). The sensor function ψ was based on normalized second derivative of electric charge distribution. The user-specified parameter ε_4 should be very small. We used $\varepsilon_4 = 0.01$. Poisson's Eq. (17) for electric potential was solved separately using and alternating-direction implicit algorithm.

NUMERICAL RESULTS

Based on this theoretical model and the numerical algorithm, a FORTRAN code was developed capable of accurately predicting convective heat transfer in EHD flows. Three different configurations have been numerically analyzed. The first configuration was a closed horizontal rectangular chamber of aspect ratio 3:1 that was discretized with a symmetrically clustered orthogonal computational grid of 60 × 30 rectangular grid cells. The chamber was 0.00275 meters in height. Non-dimensional parameters that were common to all closed container test cases were $Pr = 7.396$, $Ec = 1.28 \times 10^{-9}$, $Gr = 900$ and $Re = 30$, while those container cases that were tested with a non-zero electric field had in addition $D_E = 2.5 \times 10^7$, $S_E = 0.852$, $N_E = 1.261$ and $Pr_E = 0.0036$. The temperature difference between hot (bottom) and cold (top) walls of the container was $\Delta T = 22 \, \text{K}$.

The second test configuration represented a straight vertical channel having a width of 0.0055 meters and an aspect ratio of 4:1. It was discretized with the same number of clustered grid cells. Both computer runs with the vertical channel configuration had $Pr = 7.396$, $Ec = 2.54 \times 10^{-8}$, $Gr = 1000$ and $Re = 100$. The temperature difference between the left vertical wall (hot) and the right vertical wall (cold) was $\Delta T = 3.05 \, \text{K}$.

The third configuration was a U-shaped channel with a constant width of 0.0055 meters. The domain in this case was discretized with a clustered grid consisting of 130 × 31 grid cells. Both walls were uniformly heated and the temperature difference between the incoming fluid and the heated walls was 3.05 K. The non-dimensional parameters for this case were $Pr = 7.396$, $Ec = 2.54 \times 10^{-8}$ and $Re = 100$. A constant electric potential difference of $\Delta\varphi_o = 500$ Volts was applied between the walls of the U-shaped channel so that the electric potential non-dimensional numbers

in this test case were $D_E = 2.5 \times 10^7$, $S_E = 0.0416$, $N_E = 3.53$ and $Pr_E = 0.04$.

Closed Container

Several tests were run with this general configuration where the container was assumed filled with a neutrally charged liquid. In most tests the bottom wall acted as a uniform generator of electrically charged particles. The boundary conditions on the electric charges were specified as follows: constant electric charge distribution along the lower wall and zero normal derivative of the electric charges at the vertical walls. The charge density equation was solved at the upper wall. An external steady electric field was then imposed acting in the vertical direction by means of electrodes along the lower and the upper wall. The boundary conditions on the electric potential were specified as follows: constant (high) electric potential along the bottom wall and a constant (low) potential along the top wall and zero normal derivative of the potential at the vertical walls. Temperature was kept high and constant along the bottom wall, low and constant along the top wall, while enforcing zero normal temperature gradient on the vertical walls of the container. Pressure at all four walls was computed from the normal momentum equation pertinent to the wall in question. Fluid viscosity was treated as a constant except in one test case. Each test case was chosen to illustrate flow instability induced by the electric field (Ostroumov, 1966; Eringen and Maugin, 1990a) which is analogous to the classical Benard problem resulting in thermal buoyancy, except that here Joule heating, Lorentz force and thermal buoyancy were taken into account.

To illustrate the phenomenon of electrohydrodynamic instability, we chose the following set of non-physical non-dimensional numbers; $Pr = 1$, $Gr = 3000$, $Re = Gr^{1/2}$, $Ec = 0.0001$, $S_E = 1$, $N_E = 1$, $D_E = 1$ and $Pr_E = 1$. Strong combined thermo-electro-convection (Figure 1a) resulted in this case. Recirculation induced by the temperature gradients alone (with no electric field applied) is depicted in Figure 1b, while recirculation generated by the electrical (Lorentz) forces alone (with the entire container and the fluid kept at the same temperature) is depicted in Figure 1c demonstrating that vorticity is generated from a non-uniform electric charge distribution in a space charge loaded electric field. Electroconvective vortices analogous to thermoconvective vortices were developed since sufficient electrical potential energy was released that inverted the electrically charged layer close to the bottom wall electrode.
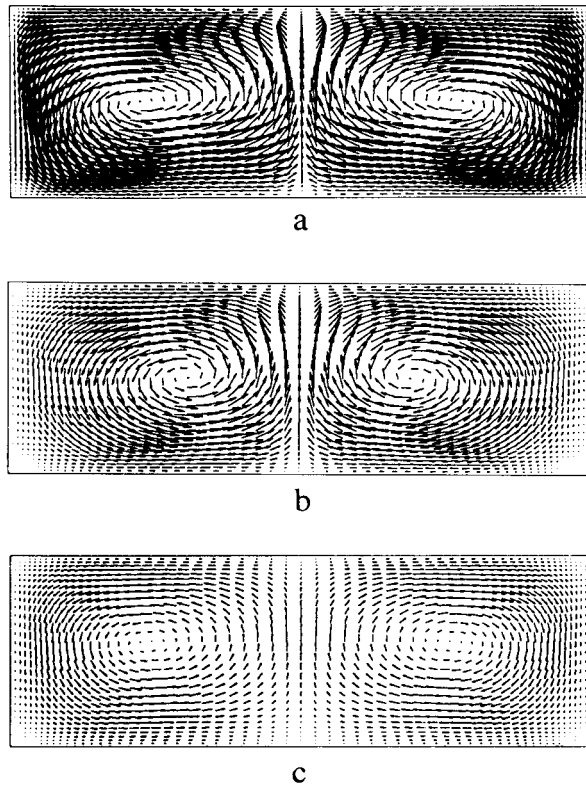
a

b

c

FIGURE 1   A demonstration of an electro-thermal convection in a closed container (top cold and bottom hot) with an electric potential difference imposed between the top and bottom. Velocity vector fields for; (a) combined thermal convection and electroconvection, (b) thermal convection alone, (c) electroconvection alone.

TABLE 1
Reference values of physical properties for fluid used

ρ_o: density	$1000\,\mathrm{kg\,m^{-3}}$
η_o: dynamic viscosity	$1.002 \times 10^{-3}\,\mathrm{kg\,m^{-1}\,s^{-1}}$
k_o: heat conductivity	$0.5682\,\mathrm{W\,m^{-1}\,K^{-1}}$
α_o: thermal expansion coefficient	$1.96 \times 10^{-4}\,\mathrm{K^{-1}}$
c_o: specific heat coefficient	$4182\,\mathrm{J\,kg^{-1}\,K^{-1}}$
b_o: electrical mobility coefficient	$5 \times 10^{-8}\,\mathrm{m^2\,s^{-1}\,V^{-1}}$

The numerical test case simulating an aqueous solution (Table 1) in a closed horizontal container was then run without an electric field and with an electric potential difference of $\Delta\varphi_o = 5600$ Volts. Figure 2a-b represent computed velocity vector fields, the velocity vectors being normalized by the reference value $v_0 = 10.9 \times 10^{-3}\,\mathrm{m\,s^{-1}}$. Maximum computed speeds in the two test runs were $0.07\,v_0$ and $0.11\,v_0$, respectively. Figure 3a–b represent the computed isotherms in the flow field and the surface heat fluxes at the top and bottom walls. The influence of the applied electric field is clearly noticeable since it generates an increased

a

b
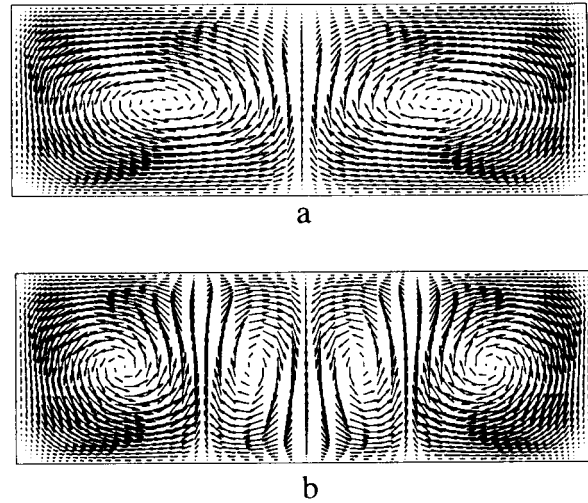
FIGURE 2   Velocity vector fields in a closed container; (a) no electric field, (b) 5600 Volts applied between the top and bottom and uniform charge injection at the bottom wall.

a

b
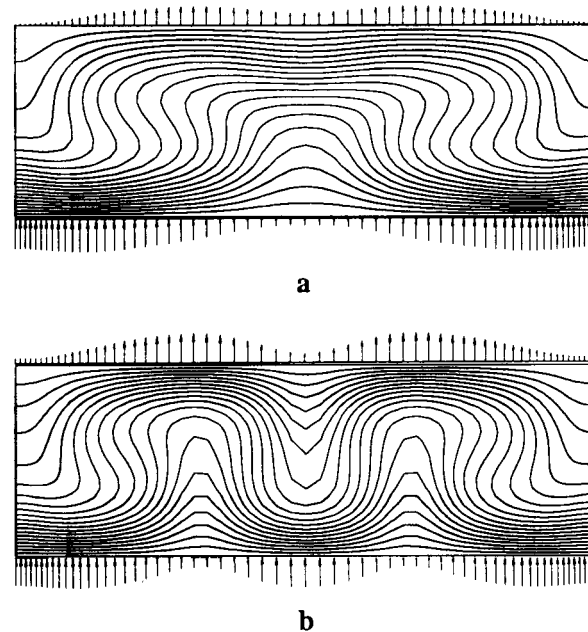
FIGURE 3   Isotherms and surface heat fluxes in a closed container (top cold and bottom hot); (a) no electric field, (b) 5600 Volts applied between the top and bottom and uniform charge injection at the bottom. (See color plate I.)

number of counter-rotating vortices. The electrically-induced secondary vortices have a destabilizing effect on the thermal boundary layer near the upper wall. Consequently, there is a redistribution of the heat fluxes computed at the bottom and the top walls when 5600 Volts are applied (Figure 3b) as compared to the

case with 0 Volts applied (Figure 3a). A 38.7% enhancement in the integrated heat transfer rate was predicted at the upper wall, compared to the case where no electric field was applied. Figure 4 depicts the computed electric potential field while Figure 5 depicts the computed charge density distribution. Notice that the electric charges are highly concentrated at the bottom wall electrode where they are being generated.

FIGURE 4   Electric potential field in a closed container (top cold and bottom hot) with 5600 Volts applied between the top and bottom and uniform charge injection at the bottom wall. (See color plate II.)
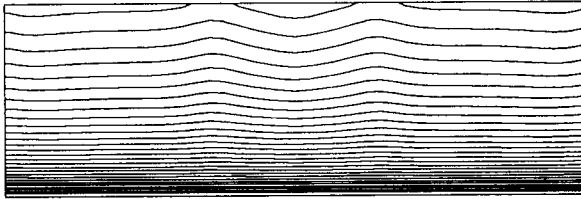
FIGURE 5   Electric charge densities in a closed container (top cold and bottom hot) with 5600 Volts applied between the top and bottom and uniform change injection at the bottom wall. (See color plate III.)
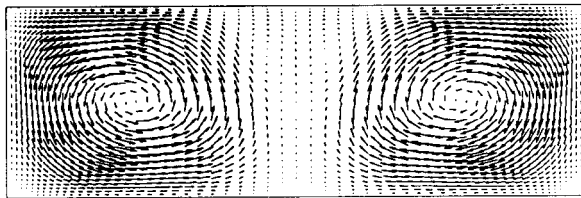
a
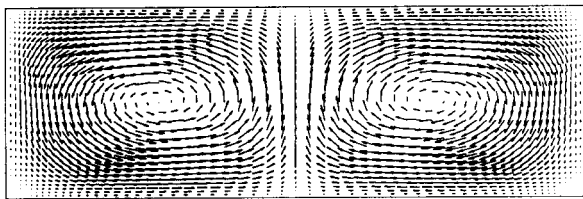
b

FIGURE 6   Velocity vector fields in a closed container with 5600 Volts applied between the top and bottom, uniform charge injection at the bottom and charge-dependent variable viscosity; (a) $(\eta/\eta_0)_{max} = 1.75$, (b) $(\eta/\eta_0)_{max} = 2.0$.

The second numerical test case was devised with the specific objective of simulating the influence of local electric charge concentration on the charged particle chaining phenomena. Fluid viscosity was modeled according to the formula $\eta/\eta_0 = 1 + C(q/q_0)^n$ where η_0 is the viscosity when there are no charged particles. Two computer runs were performed. In the first run we used $C = 0.75$ and $n = 1.25$ thus increasing the original viscosity at the locations of maximum electric charge concentration $(q = q_0)$ by 75%. In the second run we used $C = 1.0$ and $n = 1.25$ thus doubling the maximum ratio of viscosities at the locations of maximum electric charge concentration $(q = q_0)$. For this case an electric potential difference of $\Delta\varphi_o = 5600$ Volts was applied between the bottom and the top wall electrodes. The computed velocity vector fields (Figure 6a–b) and the temperature fields (Figure 7a–b) differ significantly from the case when the viscosity was assumed to be unaffected by the electric charge concentration (Figure 2a–b and Figure 3a–b). Maximum computed speeds in the two test runs were $0.045\,v_0$ and $0.05\,v_0$, respectively. The computed wall heat fluxes (Figure 7a–b) show that by neglecting viscosity's dependence on the electric charges leads to discrepancies in the prediction of EHD flows and convective heat fluxes. The effect of increasing viscosity by only 25% between the two runs is quite noticeable in the computed velocity fields since it rapidly causes suppression of an
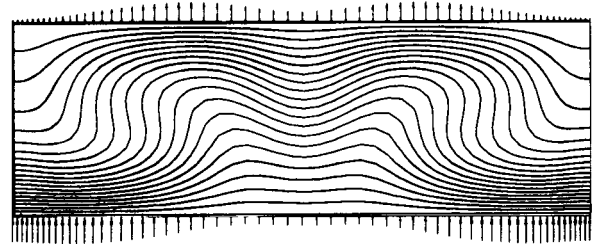
a
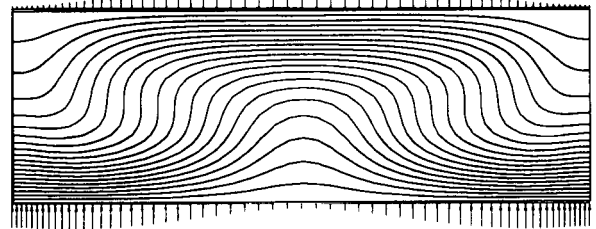
b

FIGURE 7   Isotherms and surface heat fluxes in a closed container with 5600 Volts applied between the top and bottom, uniform charge injection at the bottom wall and charge-dependent variable viscosity; (a) $(\eta/\eta_0)_{max} = 1.75$, (b) $(\eta/\eta_0)_{max} = 2.0$. (See color plate IV.)

already weak thermo-electro-convective motion. Consequently, the velocity field with $(\eta/\eta_0)_{max} = 2.0$ (Figure 7b) assumes a pattern similar to that existing in the case without an electric field when $\eta = \eta_0$ (Figure 2a).

The objective for the third numerical test was to demonstrate the influence of the variable electric charge profile as injected at the bottom wall. In this test case the aqueous solution (Table 1) viscosity was kept constant and electric charges were distributed at the bottom wall according to a sine wave. This was also a test case with a constant electric potential difference of $\Delta\varphi_o = 5600$ Volts between the bottom and the top wall electrodes. The computed velocity vector field (Figure 8a) and temperature field (Figure 8b) clearly demonstrate that both velocity and temperature fields can be actively controlled by selectively charging particles along the sections of the walls. The maximum computed speed was $0.13\,v_0$. The computed electric charges in this case are shown in Figure 8c.

Notice that the same test case with 5600 Volts applied had four counter-rotating vortices (Figure 2b) when the charges were generated uniformly instead of according to a sine wave at the bottom wall. The computed wall heat fluxes for this test case are also depicted in Figure 10b. The enhancement of integrated heat transfer rate was 63.84% as compared to the case with no electric field applied. The heat transfer enhancement rates and the distribution of heat fluxes differ substantially from the case with uniform charges imposed along the bottom wall (Figure 3b).

Vertical Channel

This numerical test case's objective was to demonstrate the influence of the applied electric field on convective heat transfer in a pressure-driven mean flow with gravity acting along the channel. The test configuration was a vertical parrallel channel with the left vertical wall uniformly hot ($\theta = 1$) and the right vertical wall uniformly cold ($\theta = 0$). The aqueous solution (Table 1)

FIGURE 8 Container with 5600 Volts applied between the top and bottom, constant viscosity and sine wave charge distribution at the bottom wall; (a) velocity vector field, (b) isotherms and surface heat fluxes, (c) electric charge densities. (See color plate V.)
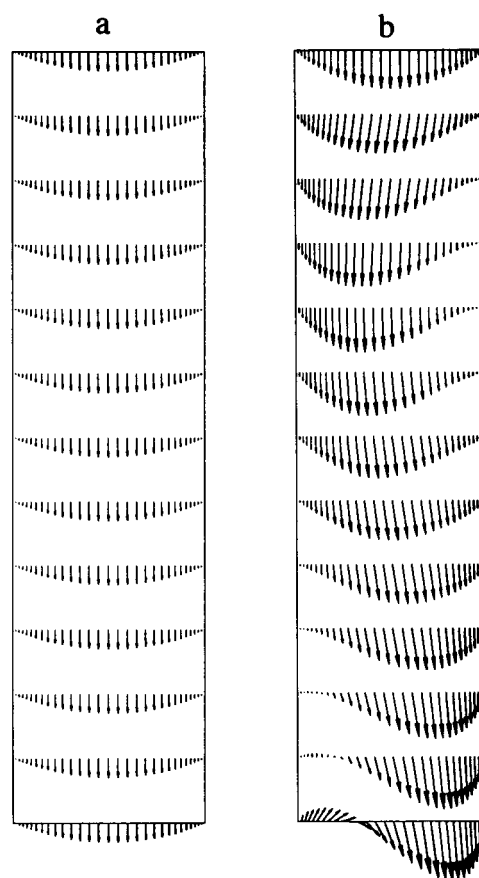

FIGURE 9 Velocity vector fields in a vertical channel; (a) no electric field, (b) 28000 Volts applied between the walls, constant viscosity and sine wave charge distribution along the left vertical wall.

having an initially uniform temperature ($\theta = 0.5$) is moving downward with an initially fully developed Poisseuile velocity profile ($Re = 100$) and a relatively small Grashof number ($Gr = 1000$). Two runs were performed with this configuration assuming constant viscosity. The first run did not involve any electric fields or charged particles and resulted in a symmetric velocity profile (Figure 9a) at the channel exit. In this test case the normalizing velocity was $v_0 = 1.8 \times 10^{-2}\,\mathrm{m\,s^{-1}}$. The computed isotherms and surface heat fluxes (Figure 10a) also indicate symmetry since the Grashof number was very small indicating negligible thermal buoyancy force. The second run was performed with a strong electric potential difference of $\Delta\varphi_o = 28000$ Volts applied between the walls resulting in the following electric non-dimensional numbers: $D_E = 2.5 \times 10^{7}$, $S_E = 2.32$, $N_E = 0.2521$ and $Pr_E = 0.00071$. Electric charges were specified along the left vertical wall as varying according to a statio-nary sine wave. The computed velocity field in this case indicates a dramatic change involving even a flow reversal (Figure 9b) at the hot wall that generated the electric charges. Maximum computed speeds in the two test runs were $1.0\,v_0$ and $1.5\,v_0$, respectively. The computed isotherms and surface heat fluxes (Figure 10b) with the electric field applied show significant perturbations as compared to the same test case with no electric field.

U-Shaped Channel

In this test case flow in a turnaround channel was investigated with the influence of an applied electric field. Both walls of the channel were heated and maintained at constant temperature ($\theta = 1.0$) while cold fluid had initially uniform temperature $\theta = 0.5$. A constant electric potential difference of $\Delta\varphi_o = 500$ Volts was maintained between the two walls of the channel with the inner wall being kept at a higher potential than the outer wall. At the inlet of the channel characteristic boundary conditions were used, that is, a parabolic velocity profile was specified along with a constant temperature. The pressure at the inlet was computed iteratively by solving the characteristic equations there (Lee, and Dulikravich, 1991a). At the exit plane, non-reflecting boundary conditions were used (Lee, Dulik-
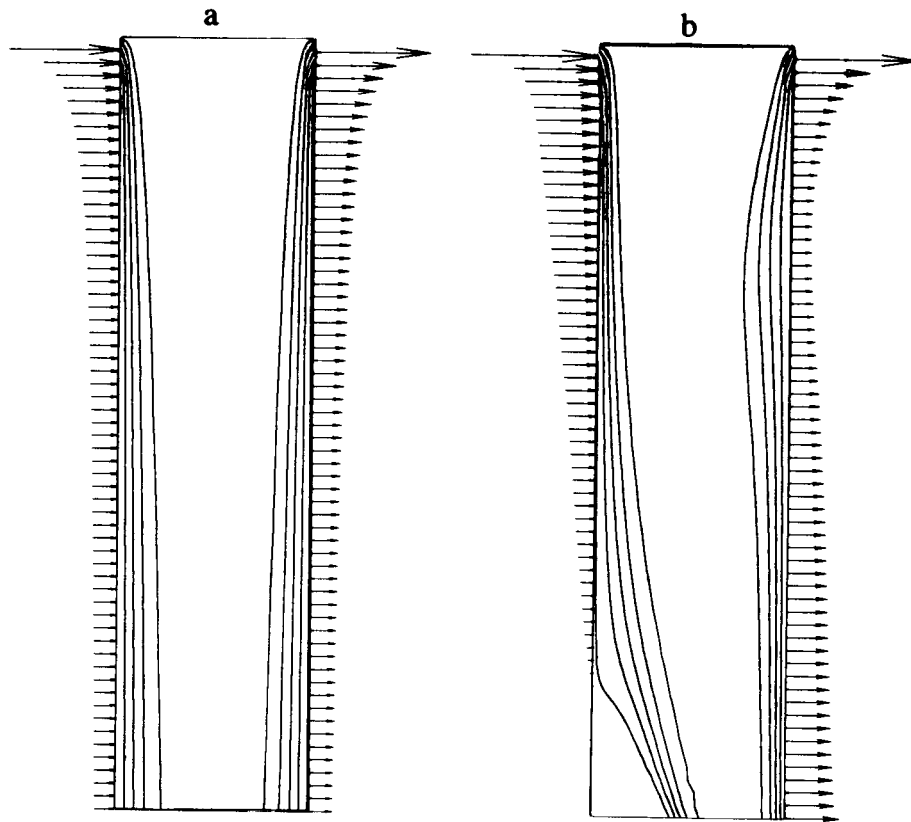

FIGURE 10 Isotherms and surface heat fluxes in a vertical channel; (a) no electric field, (b) 28000 Volts applied between the walls, constant viscosity and sine wave charge distribution along the left vertical wall. (See color plate VI.)

ravich and Ahuja, 1993) allowing for non-uniform flow at the exit since all the flow variables were computed there iteratively. The computed velocity vector field (Figure 11a) indicates a small separation zone at the end of the turnaround portion of the channel. Maximum computed speed in this test run was $1.6 v_0$. Figure 11b depicts the computed pressure distribution throughout the channel. The computed isotherms (Figure 11c) indicate the development of the thermal boundary layers at the walls of the channel. The thermal boundary layer thickens at the inner wall just after the turnaround portion, indicating the effect of flow separation on heat transfer. The computed surface heat flux distribution is shown in Figure 11d. Electric charges (Figure 11e) were injected uniformly from the turnaround portion of the inner wall only and were convected by the mean flow downstream. A slight accumulation of the charges is clearly visible in the region where flow separation occurs. Figure 11f depicts the lines of computed constant electric potential. Although uniform injection of electric charges was performed only along the turn-around section of the inner wall of the channel and a uniform external electrostatic field was applied across the channel, an overall 12% enhancement in heat transfer was predicted in this test case.
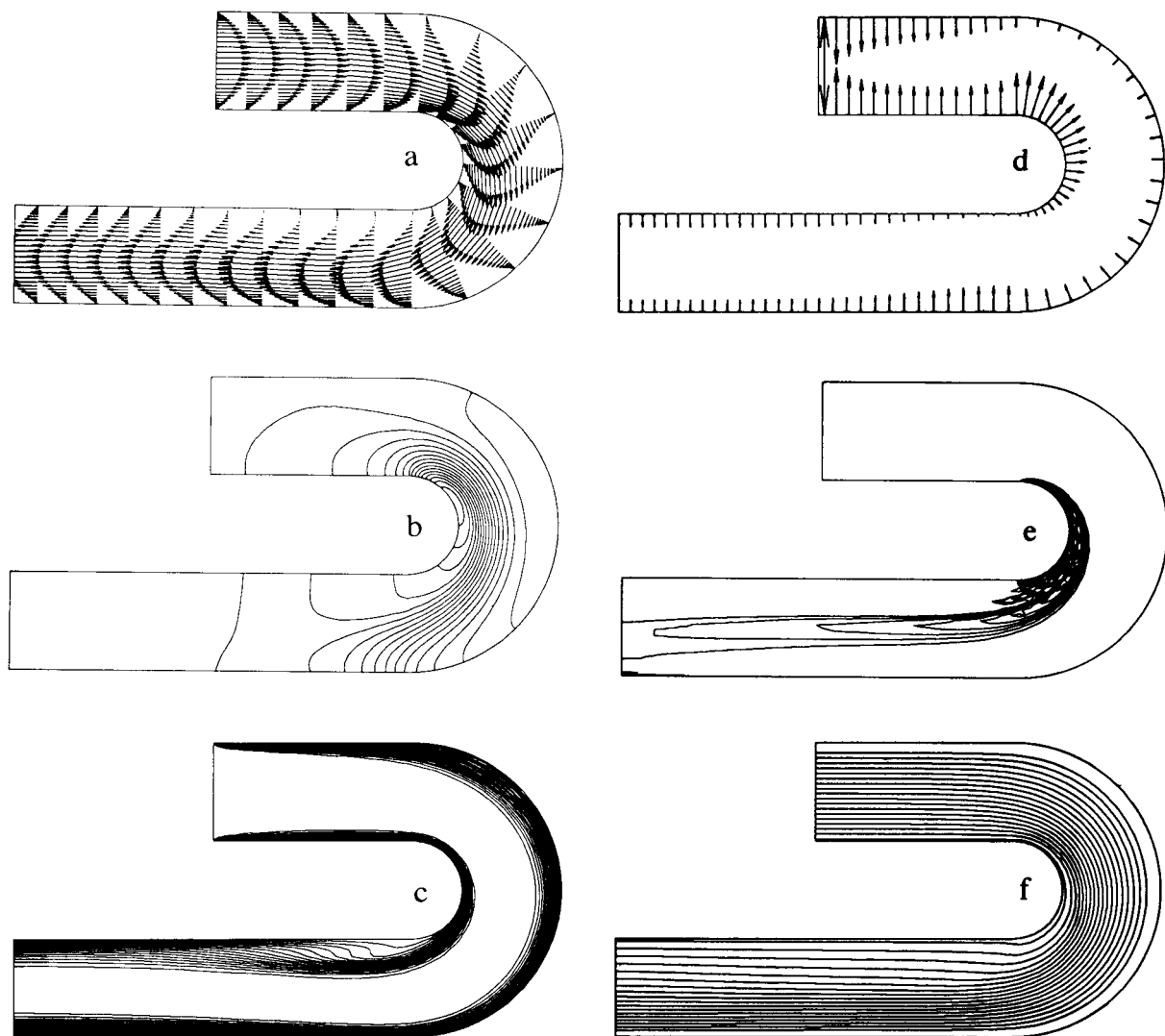
FIGURE 11   U-shaped channel with 500 Volts applied between the walls; (a) velocity vector field, (b) isobars, (c) isotherms, (d) surface heat flux distribution, (e) electric charge distribution, (f) electric potential field. (See color plate VII.)

CONCLUSIONS

A simple EHD model for a single-specie electrorheological fluid has been developed and numerically integrated for several test cases of electro-thermally generated flows in a closed container, in a vertical channel and in a turnaround channel. In all test cases a significant influence of the applied electric field acting on electrically charged particles generated at one of the solid boundaries has been demonstrated. This always resulted in a significant alteration of the flow field and consequently redistribution of the surface convective heat fluxes. when viscosity was treated as a constant, the predicted increase of the convective heat transfer rate due to EHD phenomena was between 12% and 64% for the cases studied. Importance of accounting for increased viscosity of the electrorheological fluid due to the chaining effect of the electrically charged particles has been clearly demonstrated.

These results suggest possibilities for active control and enhancement of convective heat transfer rates in electrorheological fluids by properly varying electric potential and/or the pattern of injection of charged particles at the wall electrodes.

Nomenclature

b	Charged particles mobility coefficient $(m^2 s^{-1} V^{-1})$
c	Specific heat coefficient $(m^2 K^{-1} s^{-2})$
D	Diffusivity coefficient of charged particles $(m^2 s^{-1})$
$\mathbf{D}$	Diagonal matrix
$\mathbf{E}(E_x, E_y)^T$	Electric field vector $(V m^{-1})$
$\mathbf{E}$	x-flux vector in Cartesian coordinates
$\mathbf{F}$	y-flux vector in Cartesian coordinates
$\mathbf{g}(g_x, g_y)^T$	Gravity acceleration vector $(m s^{-2})$
$\mathbf{I}$	Identity matrix
k	Heat conductivity coefficient $(kg m s^{-3} K^{-1})$
k_B	Boltzman's constant $[kg^{-1} s K]$
l	Length (m)
p	Fluid pressure $(N m^{-2})$
$\mathbf{Q}$	Solution vector in Cartesian coordinates
q	Electric charge per unit volume $(kg m^{-1} s^{-2} V^{-1})$
$\tilde{\mathbf{R}}$	Residual vector
$\tilde{\mathbf{S}}$	Source term vector
T	Temperature (K)
t	Time (s)
$\mathbf{v}(u, v)$	Velocity vector in Cartesian coordinates $(m s^{-1})$
x, y	Cartesian coordinates (m)

Greek Letters

|	
α	Thermal expansion coefficient (K^{-1})
β	Artificial compressibility coefficient
ε	Electrical permitivity coefficient $(kg m s^{-2} V^{-2})$
ε_4	Fourth order artificial dissipation parameter
η	Dynamic viscosity coefficient $(kg m^{-1} s^{-1})$
ϕ	Gravity potential $(m^{-2} s^{-2})$
φ	Electric potential (V)
ψ	Artificial dissipation sensor function
ρ	Fluid density $(kg m^{-3})$
θ	Nondimensional temperature difference

Subscripts

|	
c	Cold wall
E	Electrical
h	Hot wall
o	Reference value
$*$	Nondimensional values

References

Babskii, V. G., Zhukov, M. Y., and Yudovich, V. I., 1989. *Mathematical Theory of Electrophoresis*, (translated by C. Flick), Consultants Bureau, New York, N.Y.

Bello, M. S., and Polezhaev, V. I., 1991. Hydrodynamics, Gravitational Sensitivity and Transport Phenomena in Continuous Flow Electrophoresis, AIAA paper 91–0112, Aerospace Sciences Meeting, Reno, Nevada.

Chorin, A. J., 1967. A Numerical Method for Solving Incompressible Viscous Flow Problems, *Journal of Computational Physics*, Vol. 2, pp. 12–26.

Eringen, A. C., and Maugin, G. A., 1990a, *Electrodynamics of Continua I; Foundations and Solid Media*, Springer-Verlag, New York, N.Y.

Eringen, A. C., and Maugin, G. A., 1990b, *Electrodynamics of Continua II; Fluids and Complex Media*, Springer-Verlag, New York, N.Y.

Fernandez, J. L., and Poulter, R., 1987. Radial Mass Flow in Electrohydrodynamically-Enhanced Forced Heat Transfer in Tubes, *International Journal of Heat and Mass Transfer*, Vol. 30, No. 10, pp. 2125–2136.

Fujino, T., Yokoyama, Y., and Mori, Y. H., 1989. Augmentation of Laminar Forced Convection Heat Transfer by Application of a Transverse Electric Field, *Journal of Heat Transfer*, Vol. 111, pp. 345–351.

Gray, D. D., and Giorgini, A., 1976. The Validity of the Bousinessq Approximation for Liquids and Gases, *International Journal of Heat and Mass Transfer*, Vol. 19, pp. 545–551.

Hosseini-Sianaki, A., Firoozian, R., Peel, D. J., and Bullough, W. A., 1992. Comparative Methods for the Derivation of In Flow Electrical Characteristics of Electro-Rheological Fluids, *Journal of Intelligent Material Systems and Structures*, Vol. 3, pp. 96–111.

Jameson, A., Schmidt, W., and Turkel, E., 1981. Numerical Solutions of the Euler Equations by Finite Volume Methods Using Runge-Kutta Time-Stepping Scheme, AIAA paper 81–1259, Palo Alto, CA.

Korobko, E. V. and Mokeev, A. A., 1991. The Electrorheological Effect in Activated Suspensions, *Journal of Intelligent Material Syst. and Struct.*, Vol. 2, Jan. 1991, pp. 25–37.

Landau, L. D. and Lifshitz, E. M., 1960, *Electrodynamics of Continuous Media*, Pergamon Press, New York.

Lee, S. and Dulikravich, G. S., 1991a. Magnetohydrodynamics Steady Flow Computations in Three Dimensions, AIAA Paper 91–0388, Reno, NV; also in *International Journal for Numerical Methods in Fluids*, Vol. 13, No. 7, pp. 917–936.

Lee, S. and Dulikravich, G. S., 1991b. Performance Analysis of DMR Method for Acceleration of Iterative Algorithms, AIAA paper 91–0241, AIAA Aerospace Sciences Meeting, Reno, Nevada.

Lee, S., Dulikravich, G. S., and Kosovic, B., 1991. Electrohydrodynamic (EHD) Flow Modelling and Computations, AIAA Paper 91–1469, AIAA Fluid, Plasma Dynamics and Lasers Conference, Honolulu, Hawaii.

Lee, S., Dulikravich, G. S., and Ahuja, V., 1993. Computation of Electro-Thermo-Convective Phenomena in Electro-Rheological Fluids, ASME Fluids Engineering Summer Meeting, Symposium on Electro-Rheological Flows, Washington, D. C., June 21–24, 1993, FED–Vol. 164, pp. 29–42.

Melcher, J. R., 1981. *Continuum Electromechanics*, The MIT Press, Cambridge, MA.

Ohadi, M. M., 1991. Heat Transfer Enhancement in Heat Exchangers, *ASHRAE Journal*, Vol. 33, No. 12, pp. 42–50.

Ostroumov. G. A., 1966. Electric Convection, *Inzhenerno-Fizicheskii Zhurnal*, Vol. 10, No. 5, pp. 683–695.

Steger, J. L., and Kutler, P., 1977. Implicit Finite-Difference procedure for the Computation of Vortex Wakes, *AIAA Journal*, Vol. 15, No. 7, pp. 581–590.

Stuetzer, O. M., 1962. Magnetohydrodynamics and Electrohydrodynamics, *The Physics of Fluids*, Vol. 5, No. pp. 534–544.

Tao, R. and Sun, J. M., 1991. Three-Dimensional Structure of Induced Electrorheological Solid, *Physical Review Letters*, Vol. 67, No. 3, July 1991, pp. 398–401.

Tao, R., 1993. Phase Transition and Structure of Electrorheological Fluids, ASME Fluids Engineering Summer Meeting, Symposium on Electro-Rheological Flows, Washington, D.C., June 21–24, 1993, FED-Vol. 164, pp. 11–20.

Usman, M., Gandhi, M. V., and Kasiviswanathan, S. R., 1992. A Mixture Theory Approach for the Constitutive Modeling of Coupled Hygro-Thermo-Elastic Phenomena in Fiber-Reinforced Polymeric Composite Materials, *Composites Engineering*, Vol. 2, No. 1, pp. 21–30.

Zahn, M. and Chatelon, H., 1977. Charge Injection Between Concentric Cylindrical Electrodes, *Journal of Applied Physics*, Vol. 48, No. 5, pp. 1797–1805.
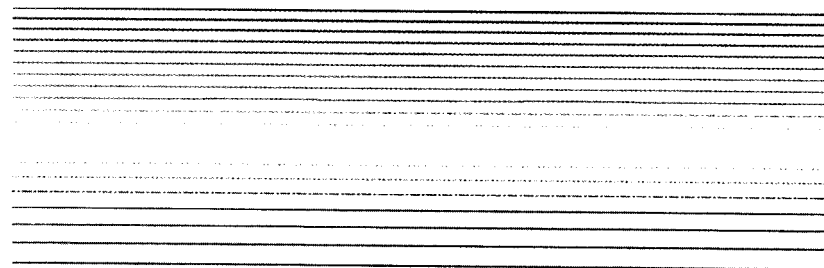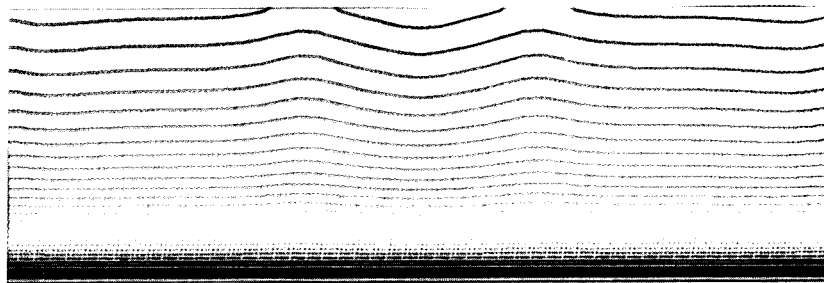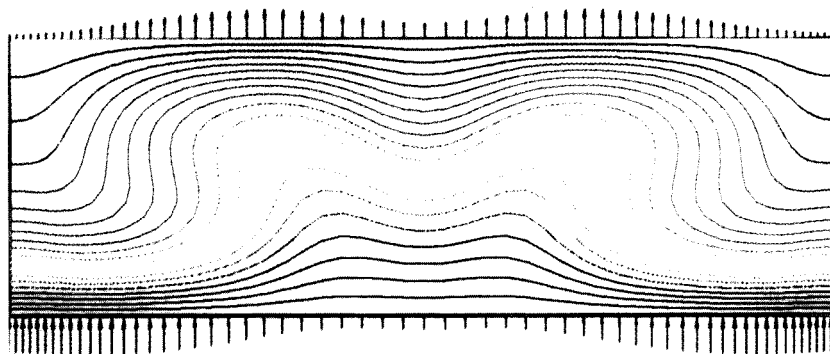
a

b
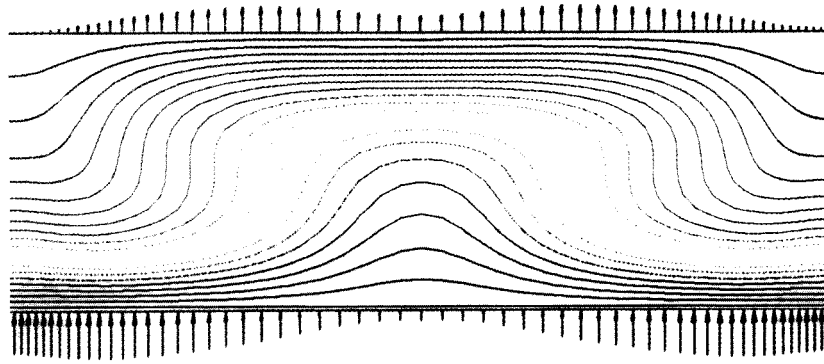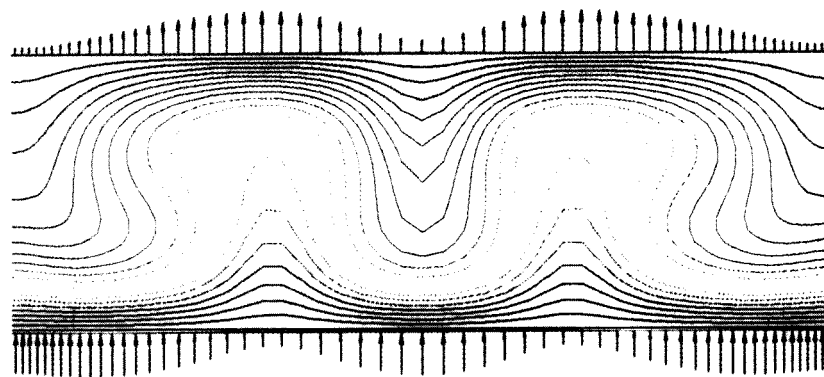
ENHANCED HEAT TRANSFER, VOLUME 1, NUMBER 1. COLOR PLATE I.
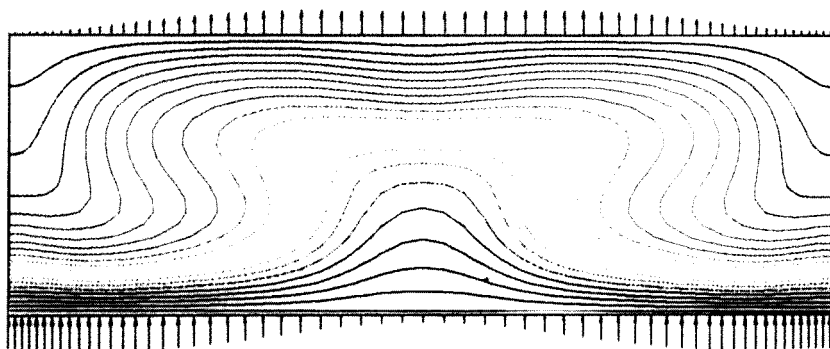See George S. Dulikravich *et al.*, Figures 3a and 3b.

ENHANCED HEAT TRANSFER, VOLUME 1, NUMBER 1. COLOR PLATE II.
See George S. Dulikravich *et al.*, Figure 4.

ENHANCED HEAT TRANSFER, VOLUME 1, NUMBER 1. COLOR PLATE III.
See George S. Dulikravich *et al.*, Figure 5.

a
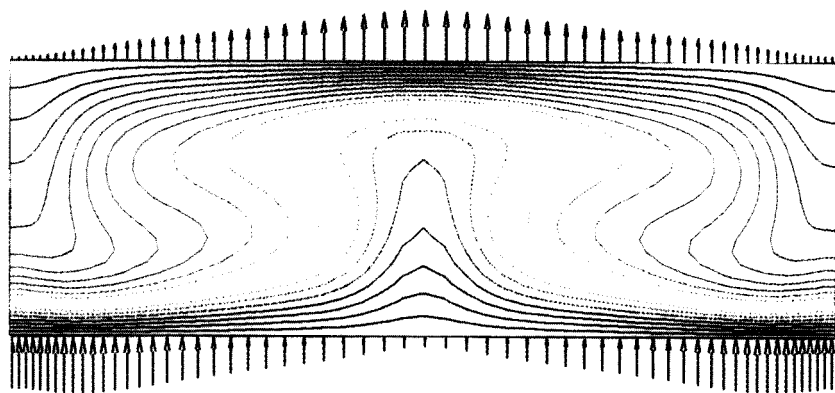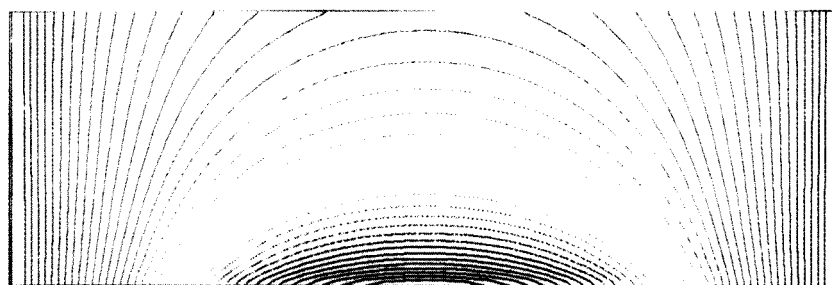
b

ENHANCED HEAT TRANSFER, VOLUME 1, NUMBER 1. COLOR PLATE IV.
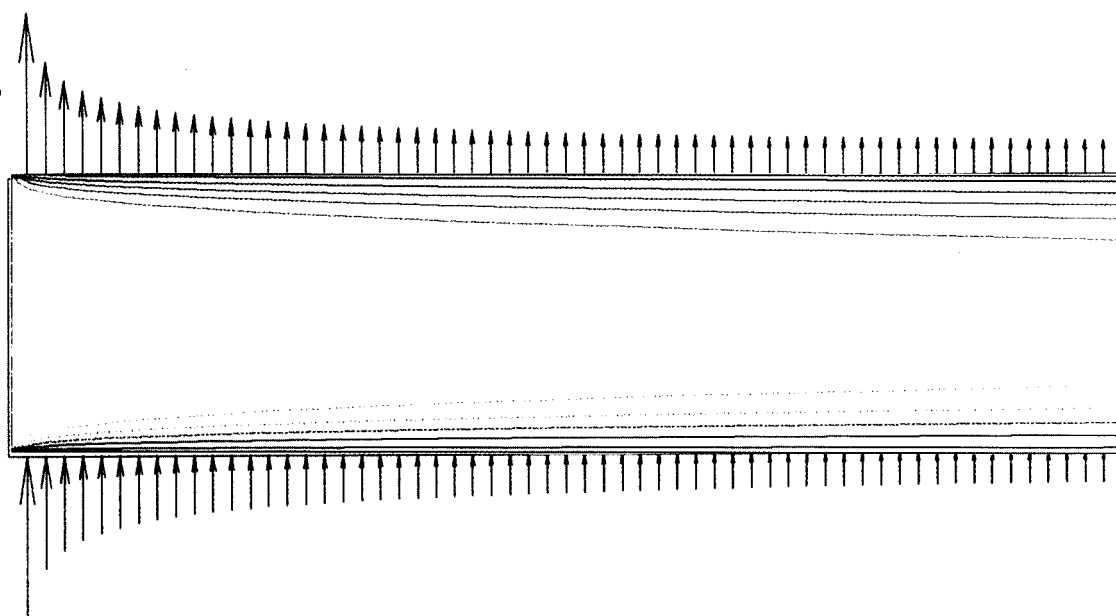See George S. Dulikravich *et al.*, Figures 7a and 7b.

b
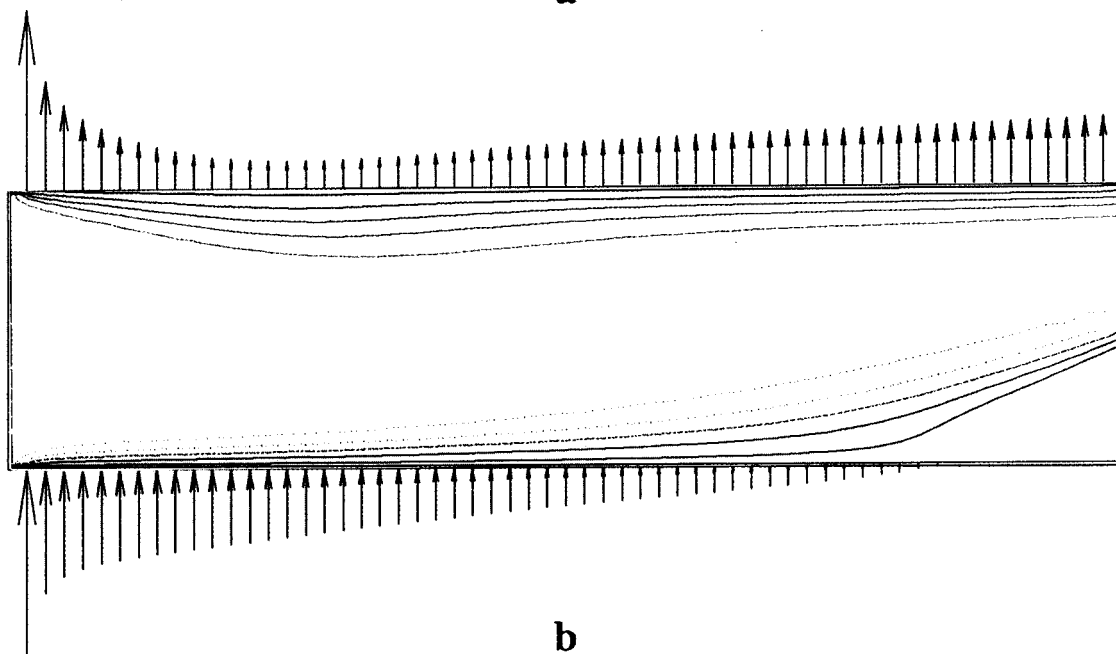
c

ENHANCED HEAT TRANSFER, VOLUME 1, NUMBER 1. COLOR PLATE V.
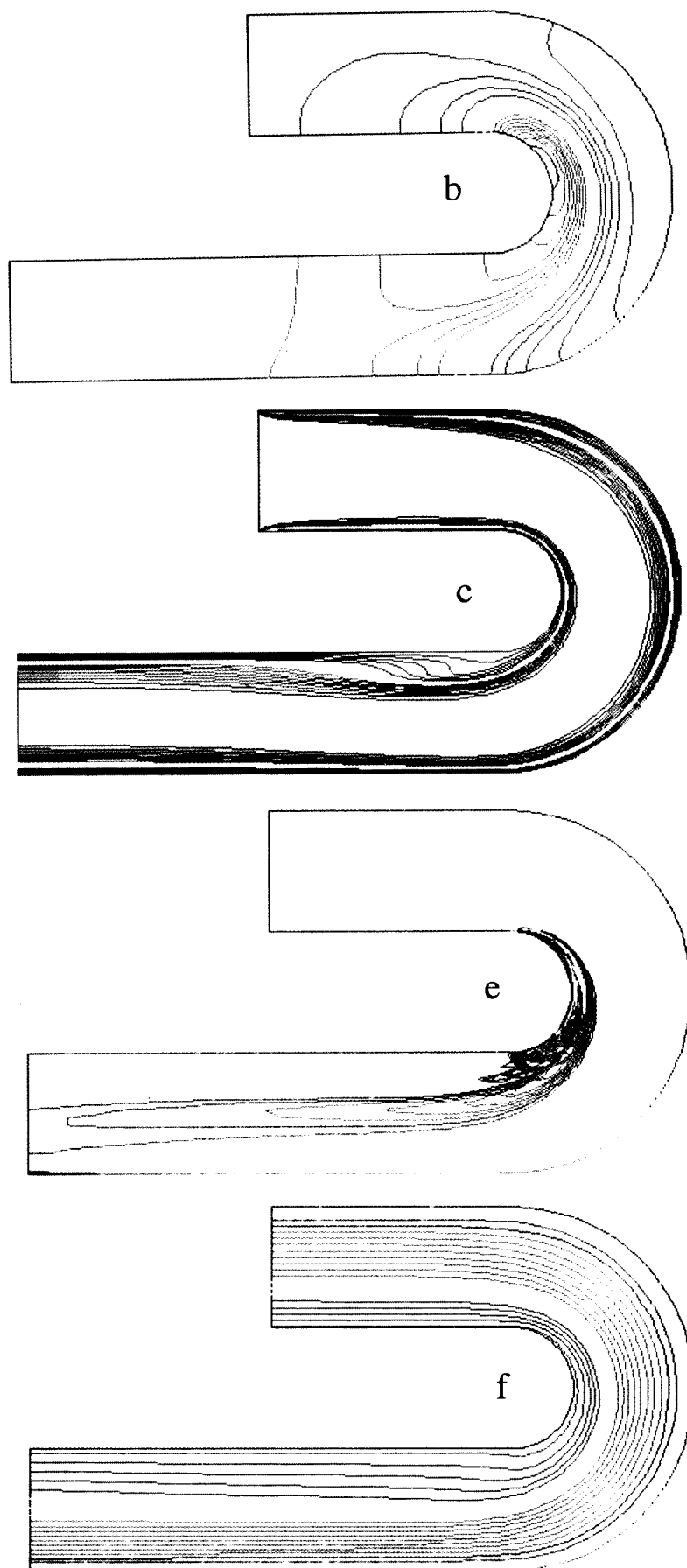See George S. Dulikravich *et al.*, Figures 8b and 8c.

a

b

ENHANCED HEAT TRANSFER, VOLUME 1, NUMBER 1. COLOR PLATE VI.
See George S. Dulikravich *et al.*, Figures 10a and 10b.

ENHANCED HEAT TRANSFER, VOLUME 1, NUMBER 1. COLOR PLATE VII.
See George S. Dulikravich *et al.*, Figures 11b, 11c, 11e, and 11f.